Residues forming the gating regions of asymmetric multidrug transporter Pdr5 also play roles in conformational switching and protein folding

Received for publication, August 27, 2022, and in revised form, October 31, 2022 Published, Papers in Press, November 10, 2022,
https://doi.org/10.1016/j.jbc.2022.102689

Maryam Alhumaidi[1,‡], Lea-Marie Nentwig[1,2,‡], Hadiar Rahman[1], Lutz Schmitt[2], Andrew Rudrow[1], Andrzej Harris[3], Cierra Dillon[1], Lucas Restrepo[1], Erwin Lamping[4], Nidhi Arya[1], Suresh V. Ambudkar[5], John S. Choy[1], and John Golin[1,*]

From the [1]The Department of Biology, The Catholic University of America, Washington, USA; [2]Institute of Biochemistry, Heinrich-Heine-Universität Düsseldorf, Düsseldorf, Germany; [3]Department of Biochemistry, University of Cambridge, Cambridge, United Kingdom; [4]Sir John Walsh Research Institute, Faculty of Dentistry, University of Ontago, Dunedin, New Zealand; [5]Laboratory of Cell Biology, Center for Cancer Research, National Cancer Institute, Bethesda, Maryland, USA

Edited by Karen Fleming

ATP-binding cassette (ABC) multidrug transporters are large, polytopic membrane proteins that exhibit astonishing promiscuity for their transport substrates. These transporters unidirectionally efflux thousands of structurally and functionally distinct compounds. To preclude the reentry of xenobiotic molecules *via* the drug-binding pocket, these proteins contain a highly conserved molecular gate, essentially allowing the transporters to function as molecular diodes. However, the structure–function relationship of these conserved gates and gating regions are not well characterized. In this study, we combine recent single-molecule, cryo-EM data with genetic and biochemical analyses of residues in the gating region of the yeast multidrug transporter Pdr5, the founding member of a large group of clinically relevant asymmetric ABC efflux pumps. Unlike the symmetric ABCG2 efflux gate, the Pdr5 counterpart is highly asymmetric, with only four (instead of six) residues comprising the gate proper. However, other residues in the near vicinity are essential for the gating activity. Furthermore, we demonstrate that residues in the gate and in the gating regions have multiple functions. For example, we show that Ile-685 and Val-1372 are required not only for successful efflux but also for allosteric inhibition of Pdr5 ATPase activity. Our investigations reveal that the gating region residues of Pdr5, and possibly other ABCG transporters, play a role not only in molecular gating but also in allosteric regulation, conformational switching, and protein folding.

ATP-binding cassette (ABC) transporters move substrates through a series of conformational changes. In the inward-facing (IF) conformation of the multidrug-exporting subfamily, which is observed in multiple X-ray and single-particle cryo-EM structures, substrates bind to residues in a large pocket with relatively high affinity. Recently, a detailed structural analysis of the TmrAB asymmetric multidrug transporter was performed under turnover conditions (1). The results from this study strongly suggest that ATP binding and dimerization of nucleotide-binding domains (NBDs) trigger a switch from the IF conformation to the outward-facing (OF, drug-releasing) conformation. ATP hydrolysis then returns the transporter to the drug-binding conformation. A comparison of structural and mechanistic properties of several ABC transporters is the subject of a recent extensive review (2).

Single-particle cryo-EM structures of the mammalian transporter ABCG2 identified Gly-553, Leu-554, and Leu-555 as part of a hydrophobic plug or gate (3) that separates the inner and outer transport substrate-binding pockets during a two-step export process. The structure of this transporter, along with that of the asymmetric ABCG5/G8 sterol transporter (4), is particularly relevant to Pdr5. Although Pdr5 is the founding member of its own subfamily of fungal ABC efflux pumps, it has a structure similar to the ABCG members, especially those that are asymmetric. Pdr5 has a characteristically reverse orientation of NBDs and transmembrane-binding domains (TMDs). The atomic structures of the mammalian ABCG family members reveal a *cis* conformation of intracellular loops and the NBD Q-loop. Thus, intracellular loop 2 contacts the N-terminal Q-loop, in contrast to members of other ABC subfamilies, where the orientation is *trans*. Although there were no crystal structures of any ABCG transporters at the time, suppressor genetics performed on Pdr5 clearly indicated a *cis* orientation for this efflux pump (5). This feature was confirmed in a recent structural study (6). Single-particle cryo-EM structures of Pdr5 in the IF and OF state were described, as well as an IF conformation with bound nucleotides and the rhodamine 6G (R6G) ligand. Pdr5 is an extreme case of ABC transporter asymmetry: all conserved sequence motifs that make up nucleotide-binding site 1 (NBS1; Walker A, Walker B, and H-loop of NBD1, as well as the C-loop of NBD2) contain amino acid substitutions of the

‡ These co-first authors contributed equally to the work.
* For correspondence: John Golin, golin@cua.edu.
Present addresses for: Hadiar Rahman, Laboratory of Cell Biology, Center for Cancer Research, National Cancer Institute, Bethesda, MD 20892; John Golin, Department of Biology, Stern College for Women, Yeshiva University, 215 Lexington Ave, New York, New York 10,016.

catalytically relevant residues (discussion in Golin and Ambudkar, 7). Thus, one NBS is incapable of significant ATP hydrolysis (8). The asymmetry is also reflected in the structures. NBS1 contains either no nucleotide or ATP, while the active NBS, NBS2, contains ADP in the IF conformation or ADP*V_i in the OF state. In all the structures examined, only a *cis* interaction between one NBD and one TMD is present in the structures, only one coupling helix per TMD is present, and the domain swapping seen in structures of the ABCB subfamily is absent. Interactions occur between coupling-helix 1 (the loop between transmembrane-helix 2 (TMH2) and TMH3) and the Q-loop of NBD1 and on the opposite site of the protein between coupling-helix 2 (the loop between TMH8 and TMH9) and the Q-loop of NBD2. It is primarily TMD1 that undergoes changes during the switch from IF to OF that underlies the transport cycle. This switch results in a peristaltic motion that squeezes out the bound substrate from its binding site in the IF conformation into the exit channel and releases the substrate at the outer leaflet–extracellular space interface. This suggests that substrates are not released into the aqueous medium but rather repartition into the outer leaflet of the membrane (9, 10).

The reduction in substrate affinity of the OF conformation is not enough to preclude reflux of substrates following expulsion. For example, the reduction in binding affinity measured in P-glycoprotein (P-gp) was only about 30-fold (11). Partly because of this observation, a gate or molecular diode was proposed for ABC transporters (12). The first functional evidence for a molecular diode was described in the yeast multidrug transporter Pdr5 and the mammalian TAP antigen transporter (13, 14). Mehla *et al.* (13) demonstrated that a serine-1368-alanine (S1368A) mutation in Pdr5 was hypersensitive to all tested xenobiotic compounds relative to an isogenic WT strain, even though the mutant had no defect in plasma membrane (PM) localization, intradomain signaling, drug binding, or ATPase activity. However, considerable reflux of R6G occurred during transport. Elegant work with the TAP transporter demonstrated a gating function that required the D-loop and presumably the same signal transmission pathway used to ferry processed antigen peptides (14). This D-loop mutant converted TAP from an active transporter into a facilitator.

In this study, we further explored the features of the Pdr5 extrusion gate. Ser-1368 lies in the middle of TMH-11, which is split into three separate helices and lines the R6G-binding site. Ser-1368 is in TMH11a, while TMH11c crosses over to the second extracellular domain-2, which contains two conserved disulfide bridges. When the structures of Pdr5 and ABCG2 are superimposed, Ser-1368 is near the Leu-554 and Leu-555 plug. The ABCG2 gate also includes Gly-553. The residues in Pdr5 corresponding to the two Leu residues are Val-1372 and Met-1373 (Fig. 1*A*). A bioinformatic analysis of the Pdr subfamily (15) demonstrated that amino acids in this vicinity are highly conserved (Fig. 1*B*). These include Phe-1369, Gly-1371, Val-1372, and Met-1373. Val-1372 and Met-1373 are the first two residues in extracellular loop 6. We also made an alignment between ABCG2 and 17 other members of the ABCG subfamily with 41% to 73% amino acid identity. The residues corresponding to Phe-1369 and Gly-1371 of Pdr5 are also highly conserved. Both residues were present in 16 of the 17 sampled ABCG sequences.

A similar set of residues in the N-terminal half of Pdr5 extends from Tyr-680 to Ile-685 (Fig. 1*C*). Residues Gly-682, Phe-683, and Ala-684 are equivalent to Gly-1371, Val-1372, and Met-1373. Ala-684 is not conserved in the pleiotropic drug resistance (PDR) subfamily of ABC transporters. Immediately adjacent is the highly conserved Ile-685 residue.

This study analyzes the role of these amino acids in Pdr5. The Pdr5 gate is asymmetric. In contrast to ABCG2, four rather than six residues are involved. Furthermore, our results suggest that gate region residues play a variety of roles, including conformational switching, protein folding, and molecular gating. Surprisingly, some of the residues in the molecular gate region modulate allosteric inhibition of the Pdr5 ATPase activity by its transport substrates.

Results

Single-molecule cryo-EM structures of the Pdr5 extrusion gate

The location of the ligand-binding site and the residues of Pdr5 corresponding to the Leu gate of ABCG2 as well as Ser1368, which is part of the molecular diode, are shown in Figure 2.

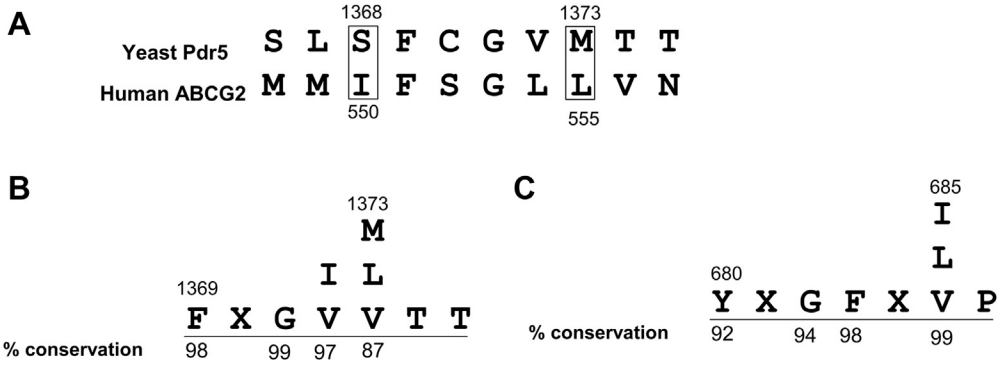

Figure 1. Residues of the Pdr5 extrusion gate region are highly conserved. *A*, an alignment of Pdr5 with the human half-transporter ABCG2 was performed using the ExPASy bioinformatics database. *B*, a bioinformatic analysis of 263 PDR subfamily members by Lamping *et al.* (15) was used to evaluate the conservation of the residues that are adjacent to Ser-1368. An X indicates a nonconserved residue. *C*, the amino acids in the amino terminal half of Pdr5 corresponding to the Ser-1368 region are indicated in a similar manner.

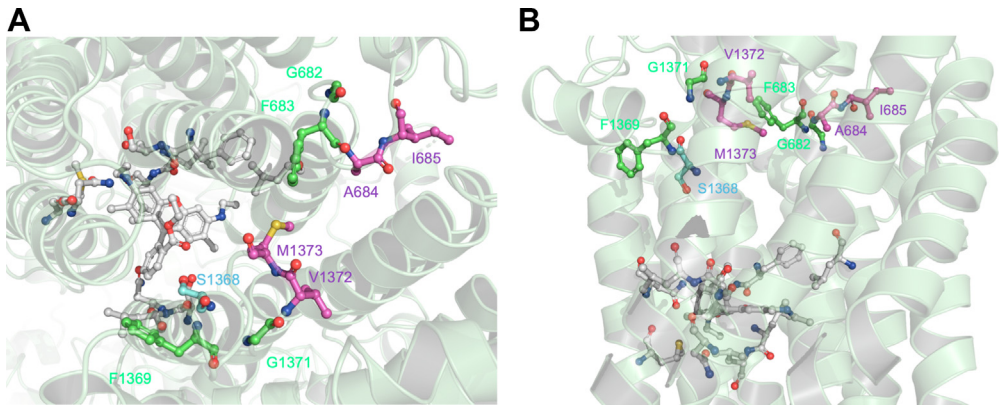

Figure 2. Structure of the extension gate in the inward-facing (IF) conformation. This image was constructed from a cryo-EM image of 3.1 Å resolution. The views are (*A*) from the extracellular side (*top*) into the ligand-binding site of Pdr5 in the IF state and (*B*) a lateral view from the membrane. Residues of the gate and the gating region (Gly-682, Phe-683, Ala-684, Ile-685, Gly-1371, Val-1372, and Met-1373) are in *magenta*, the molecular diode-region residue Ser-1368 is in *cyan*, and those amino acids (*gray*) interacting with the bound ligand R6G are highlighted in *ball* and *sticks* representation. Amino acids analyzed in this study are shown as *green ball* and *sticks*. R6G, rhodamine 6G.

The spatial relationships between the residues in the region of the gate are revealing. The three images in Figure 3 provide the perspective from above the extracellular space. The first picture (Fig. 3*A*) is a close-up view of these residues in the IF (*gray*) and OF (*cyan*) conformations, respectively. During conformational switching, the residues in amino terminal half of Pdr5 (Gly-682, Phe-683, Ala-684, Ile-685) barely move. In contrast, the residues of the carboxyl terminal half undergo significant shifts in location. The Met-1373 side chain, for instance, moves further away from the amino terminal residues and the Ser-1368 side chain moves further away from Met-1373. The result of this movement is clearly seen when comparing the IF (Fig. 3*B*) with the OF (Fig. 3*C*) surface structures in which Phe-683, Ala-684, Ile-685, Val-1372, and Met-1373 are highlighted as spheres. The gate proper comprises Gly-682, Phe-683, Gly-1371, and Met-1373. In the IF conformation, the gate is completely closed by the single pair of interacting hydrophobic residues, Phe-683 and Met-1373. The striking asymmetry of Pdr5 is apparent because bioinformatic data suggest a similar interaction between Val-1372 and either Ala-684 or Ile-685, which is not observed. The closest that Ile-685 gets to a residue on the opposite side of the efflux channel is a 7.1 Å distance from Met-1373 (Fig. S1). This is notably different from the homodimeric ABCG2 gate, where Leu-554 and Leu-555 from each side create a hydrophobic plug. When Pdr5 is in the OF conformation (Fig. 3*C*), the channel space is 11 Å. Because a benzene ring is roughly 2.8 Å in diameter and effective Pdr5 transport substrates are always larger than this (16), it seemed possible that the transport substrates could be in contact with the gating residues during efflux, a conclusion strongly supported by data obtained in this study.

As noted in the recent Pdr5 structural study (6), an implied peristaltic movement during conformational switching results in extrusion of transport substrates.

Characterization of F683L, A684S, and M1373T mutants originally isolated by their altered FK506 resistance

A topology diagram showing the location of all the mutant residues analyzed in this study is found in the supporting information (Fig. S2). When we began our analysis of the Pdr5 gating region, we used a combination of bioinformatics from fungal PDR transporters and the published structure of the ABCG2 multidrug transporter to identify conserved residues Gly-682, Ile-685, Gly-1371, Val-1372, and Met-1373 as components of the Pdr5 molecular gate. We performed alanine-scanning mutagenesis to create the G682A, I685A, G1371A, V1372A, M1373A, and I685A, V132A double-mutant substitutions, which we compared to an isogenic WT control strain.

It was not until much later that reexamination of the structures revealed the critical importance of Phe-683. Remarkably, F683L, A684S, and M1373T mutants were in a genetic background closely related to the one used in this study. These were previously identified as part of a genetic screen for mutants conferring FK506-resistance to fluconazole transport (17). In that study, these mutants exhibited hypersensitivity to at least some Pdr5 transport substrates. Therefore, we characterized these mutants with similar methods to those used for the others in this study. Because these critical mutants were not alanine substitutions and our methods had minor differences, we present these results first in a separate section.

In the original characterization of these strains, the F683L mutant was profoundly hypersensitive to R6G; its minimum inhibitory concentration was just one-eighth of the WT value. It was also hypersensitive to cycloheximide and fluconazole. The A684S and M1373T mutants were also hypersensitive to some of the drugs, but their phenotypes were mild relative to the F683L strain. The *PDR5* gene in these strains was resequenced to verify the presence of the mutation of interest. Purified PM vesicles were prepared from these strains. A Coomassie blue–stained gel and Western blots of the vesicles indicated equivalent levels of Pdr5 in all of the preparations (Fig. S3, *A* and *B*). The ATPase activity was also examined. All of the mutants had activities that were similar to the WT control (Fig. S3*C*). We evaluated the sensitivity of the mutant ATPases to clotrimazole, which is known to be an allosteric inhibitor of this activity (18–20). The inhibition curves of the

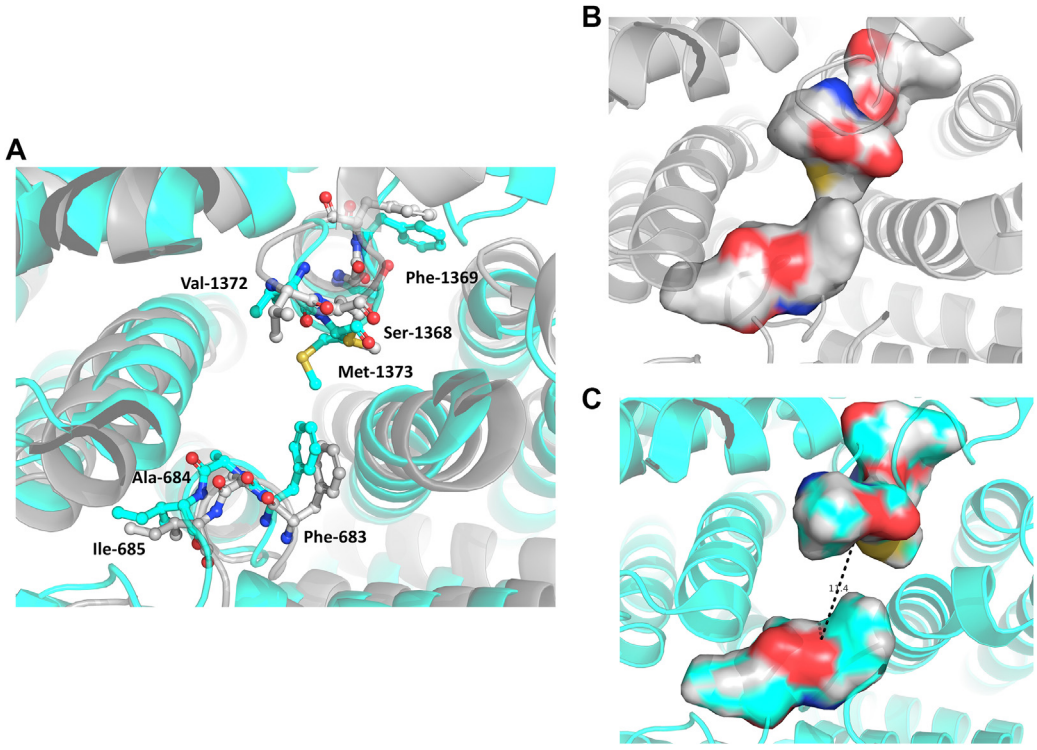

Figure 3. Zoom and surface illustrations of the gating residues in the IF and OF conformations. In all the images, the viewer is looking down from the extracellular space. *A*, a zoom-in image of the residues making up the extrusion gate region. The positions of the residues are shown in the IF (*gray*) and OF (*cyan*) conformations. *B*, a surface illustration showing the interaction between Phe-683 on the *left side* of the channel and Met-1373 on the *right side* in the IF conformation. *C*, the same arrangement is shown for the OF conformation. The IF image comes from a structure of 3.1 Å resolution; the OF from one at 3.9 Å resolution. IF, inward-facing; OF, outward-facing.

mutant enzymes were not significantly different from the WT plot, with IC_{50} values of 2.0 to 2.8 μM (Fig. S4). These values, in turn, were much like the one reported previously for the WT enzyme, 2.2 μM (21).

In light of these results, we reexamined the relative resistance of the mutants to the drugs used in the original study (Fig. 4). The F683L mutant exhibited significant hypersensitivity to all four drugs. It was 2× to 4× more sensitive than the

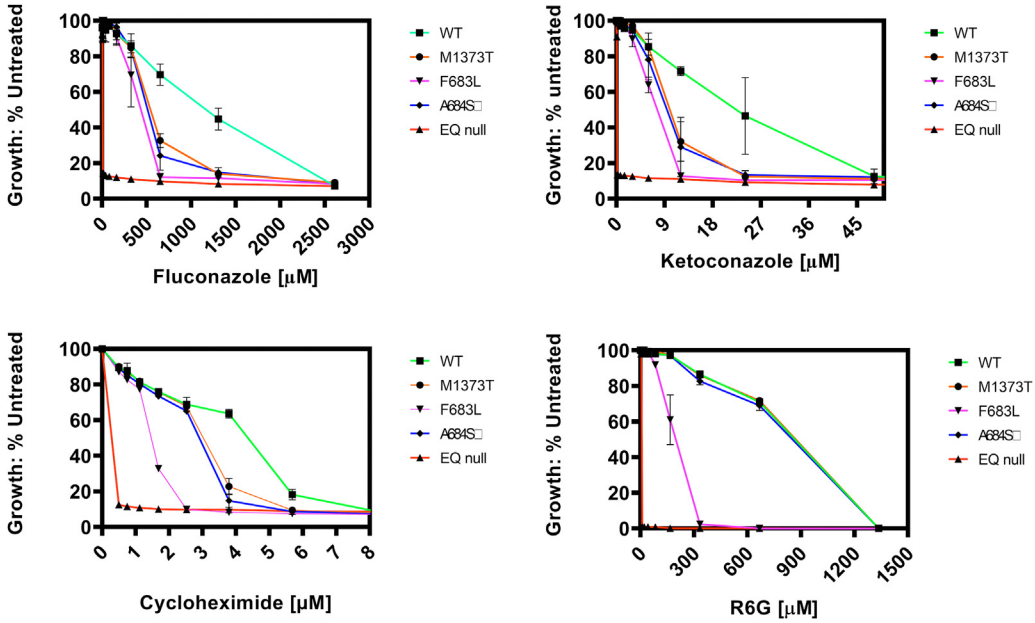

Figure 4. Relative resistance of mutant and WT strains to four Pdr5 transport substrates. Assays of relative resistance to cycloheximide, R6G, ketoconazole, and fluconazole were performed as previously described (31). In these experiments, n = 4 and a Pdr5 null mutant containing a mutation in the catalytic carboxylate of the catalytic ATP site and the corresponding glutamine in the deviant ATP-binding site serves as the negative control. R6G, rhodamine 6G.

WT. The F683L mutant was most sensitive to R6G and least sensitive to ketoconazole. The M1373T and A684S mutants were nearly identical in phenotype, which was drug specific. They were mildly hypersensitive to cycloheximide but quite hypersensitive to ketoconazole and fluconazole. Remarkably, their resistance to R6G was indistinguishable from the WT, even though the substitution of a polar residue for a nonpolar one occurred at each position.

The F683L mutant is profoundly deficient in R6G transport

Transport of R6G in PM vesicles was measured with a well-established assay (22). PM vesicles were incubated in the presence of R6G and ATP. Transport in this type of experiment is measured against a concentration gradient of R6G (Fig. 5*A*). Although the WT vesicles exhibit quenching kinetics much like those described previously (8, 21), the F683L mutant had a nearly null phenotype with little reduction in fluorescence signal.

The diode-malfunctioning mutant S1368A exhibited a unique transport phenotype. It was profoundly transport deficient in an assay of efflux in whole cells against a concentration gradient of R6G. Thus, when transport was conducted for 90 min in the presence of R6G, the S1368A mutant accumulated 5× to 10× more fluorescence than did the WT. This was shown to be directly attributable to drug reflux. In contrast, when we performed a whole-cell transport assay in the direction of the gradient so that R6G was diluted in the extracellular buffer, the mutant phenotype was nearly WT (10). We tested the F683L mutant in analogous fashion. To do this, log-phase cells were preloaded in Hepes buffer with 20 μM R6G and no additional glucose for 90 min. Under these conditions, cells continue to transport R6G until the internal pool of glucose is severely diminished, at which point R6G (as well as fluorescence) accumulates. The WT strain, though, always accumulates less fluorescence than any transport-deficient mutants. That is also the case in the present study (Fig. 5*B*). Thus, the ΔPdr5 strain (AD1-7) retained the most fluorescence and the F683L mutant accumulated about 3× as much as the WT control.

However, when transport was conducted in the direction of an R6G gradient, the F683L mutant performed robust drug efflux (Fig. 5*C*). In fact, under these conditions, this mutant seemed modestly better than the WT at clearing R6G. A two-way ANOVA test indicated that the WT and F683L mutant curves were significantly different. The p value for all fixed effects was <0.001. We do not have an obvious biochemical explanation for this. It is possible that a minor genetic change unrelated to Pdr5 took place in the F683L strain that accounts for the slightly better transport kinetics.

Expression of alanine substitution mutants in purified PM vesicles

We also constructed a series of alanine substitution mutations in conserved residues in the gating region of the N- and C-halves of Pdr5. The G682A, I685A, F1369A, G1371A, V1372A, and M1373A mutations were made as previously described (5). We also made an I685A, V1372A double mutant.

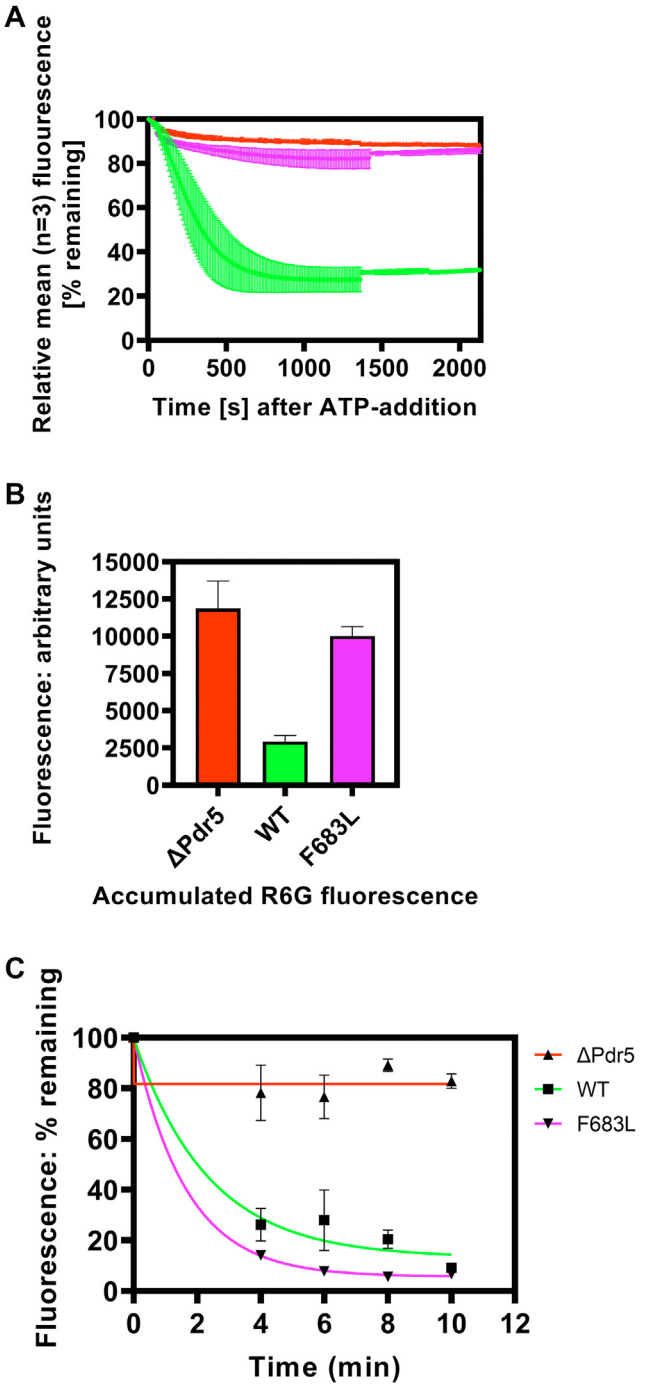

Figure 5. The F683L mutant is defective in transport of R6G against a concentration gradient. *A*, an R6G, fluorescence quenching assay was performed with PM vesicles as previously described (8) using 30 ng PM vesicle protein, 5 mM ATP, and 150 nM R6G. The shaded region indicates the SD. *B*, accumulation of R6G prior to glucose-mediated efflux. Log-phase cells were incubated in 0.2 M Hepes buffer plus 20 μM R6G at 30 °C for 90 min. In these experiments, n = 3. *C*, the transport capability of the F683L mutant in the direction of 20 μM R6G was measured as described in the Experimental procedures. In these experiments, n = 5. *B*, Western blotting was performed as described by Rahman *et al.* (33) using 5 μg of solubilized PM vesicle protein following gel electrophoresis that was performed as described in the Experimental procedures. PM, plasma membrane; R6G, rhodamine 6G.

PM vesicle preparations were made from all these strains. A Coomassie-stained gel and a Western blot of the solubilized PM vesicle proteins were prepared (Fig. S5).

The Coomassie blue–stained gel of the membrane preparations (Fig. S5*A*) indicated equivalent loading of the samples (see, for example, the Pma1 band). The presence of a highly expressed Pdr5 band was present in six of the nine samples. Densitometry revealed that the PM vesicles prepared from the I685A, V1372A, and double-mutant strains have about twice the amount of Pdr5 protein as the WT. We further confirmed this observation in a second set of preparations from the WT and double-mutant strains. The Western blot substantiated these observations (Fig. S5*B*). No Pdr5 protein was observed in samples from the ΔPdr5, G682A, and M1373A strains. The failure of the M1373A protein to localize to the PM membrane mirrors the behavior of its equivalent L555A mutant residue in ABCG2 (7).

The G1371A PM vesicle preparations had reduced ATPase activity

We also evaluated ATPase activities in the mutants. The ATPase activity of Pdr5 follows standard Michaelis–Menten kinetics, and representative plots are illustrated in Figure 6*A*. The V_{max} of the F1369A mutant, although on the lower end (1.8 μmol min^{-1} mg^{-1}) is nevertheless within the range of activities seen for WT activities (2.5 μmol min^{-1} mg^{-1} in this plot). The G1371A activity (0.9 μmol min^{-1} mg^{-1}), however, was about one-third the WT value. We also assayed two independent PM vesicle preparations for each strain at the single concentration of 3 mM ATP. The WT and F1369A mutant activities were 2.0 ± 0.4 and 1.4 ± 0.3 μmol min^{-1} mg^{-1}, respectively. A *t* test indicated that these activities were not significantly different (p = 0.1429). The average activity from the G1371A mutant enzyme (0.6 ± 0.2 μmol min^{-1} mg^{-1}) was, however, significantly lower than the WT (p = 0.0407). When we assayed the ATPase activities of the I685A, V1372A, and double-mutant PM vesicle preparations (Fig. 6*B*), the activities of the single mutants and double mutants were higher than the WT values. The elevated ATPase activities in these mutants almost certainly reflect the higher level of their Pdr5 protein in the PM vesicles.

The allosteric site for substrate-mediated ATPase inhibition overlaps the Pdr5 gate region

We tested the sensitivity of the alanine substitution mutant ATPases to inhibition by clotrimazole. Representative plots indicated that PM vesicles made from the G1371A mutant exhibited striking hypersensitivity to this transport substrate (Fig. 6*C*). Analogous results were obtained when bifonazole was used as an inhibitor (Fig. 6*D*).

Markedly, different results were obtained with the single I685A and V1372A mutants and an I685A, V1372A double mutant. With clotrimazole as the inhibitor, the single mutants had IC_{50} values roughly 1.5× as high as the WT (Table 1). The double-mutant ATPase, however, was significantly more resistant than the single mutants' enzymes. Testing of a second

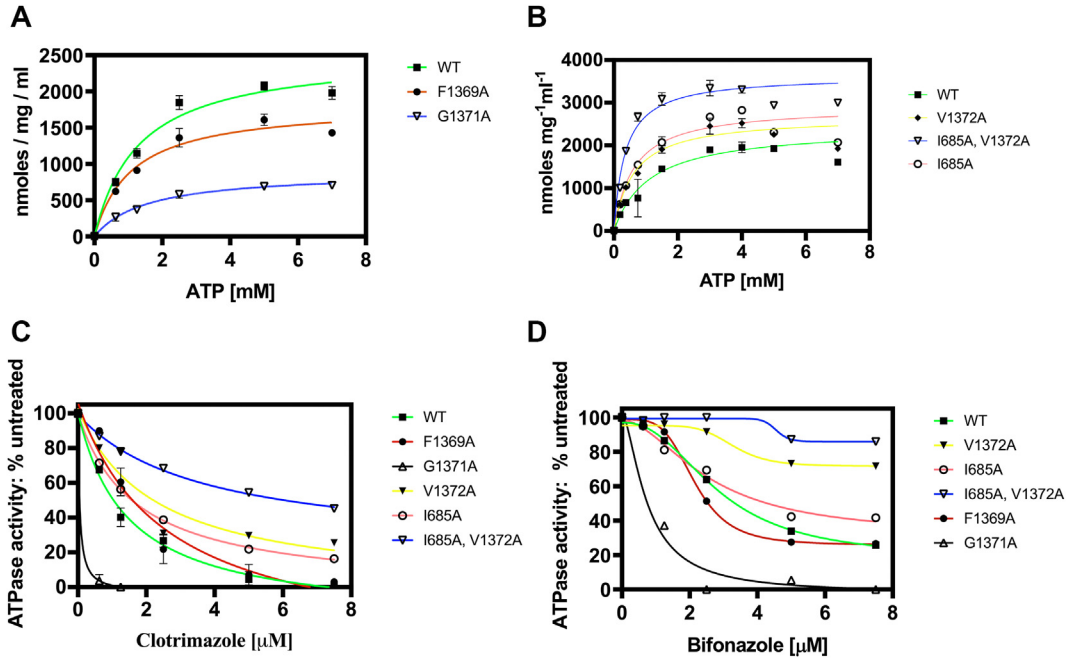

Figure 6. The Ile-685 and Val-1372 residues are part of an allosteric inhibition site. *A*, the ATPase activity was measured at multiple concentrations of ATP. Assays were performed in Tris-glycine buffer (pH 9.5) with 2.5 μg of purified PM vesicle protein at 35 °C for 8 min in a circulating water bath as described in the Experimental procedures. Representative plots of WT, F1369A, and G1371A PM vesicle proteins are shown, and similar results were obtained with additional preparations of WT, F1369A, and G1371A PM vesicles. *B*, assays analogous to those in panel (*A*) were carried out with PM vesicle preparations from the I685A, V1372A, and I685A, V1372A double mutant strains. *C*, inhibition of ATPase activity by clotrimazole and (*D*) allosteric inhibition by bifonazole was evaluated using the same conditions described in panel (*A*), except varying concentrations of clotrimazole were added to different reaction tubes containing 3 mM ATP. For the F1369A, G1371A, and the I685A, V1372A double mutant, each plot represents the average values of two PM vesicle preparations. PM, plasma membrane.

preparation of double-mutant vesicles verified these results. In this experiment, we also used higher concentrations of these inhibitors to get better estimates of the IC_{50} values (Fig. S6). The double-mutant value (6.3 μM) for clotrimazole was 5× as much as the WT and therefore greater than the sum of the single values. A similar phenomenon was observed with bifonazole. In this case, the single mutant IC_{50} values were not significantly different from the WT. The double mutant, however, had an IC_{50} 4.5× as great. These results suggest that Ile-685 and Val-1372 are part of a site-mediating allosteric inhibition of Pdr5 ATPase activity by its transport substrates. These data are consistent with our previous observations that neither the ATP-binding sites nor the drug-binding sites in the binding pocket are the location of inhibition (18).

The sensitivity of the F1369A mutant ATPase resembled that of the WT, and a two-way ANOVA test indicated that the curves were not significantly different (p = 0.1326.)

The F1369A and G1371A mutants are hypersensitive to all five tested Pdr5 substrates

We used both the WT and ΔPdr5 strains as controls to evaluate the relative resistance of the mutants to five Pdr5 substrates. The list of their properties in Table S1 demonstrates the diverse chemical nature of these compounds.

We evaluated resistance to aromatic and nonaromatic substrates. The range in molecular volume is significant as is the solubility in octanol *versus* water (logP). Figure 7 contains the results for the F1369A, G1371A, and the original S1368A diode mutant strains. Results for I685A, V1372A, and the double I685A, V1372A mutant are shown in Figure 8. As expected, the M1373A mutant is phenotypically indistinguishable from the ΔPdr5 control strain in resistance to cycloheximide and climbazole. The F1369A and G1371A mutants exhibited a similar hypersensitivity to all the compounds, as found in the original diode mutant S1368A. The F1369A and G1371A mutants were more sensitive than the WT control to all the drugs but more resistant than the isogenic ΔPdr5 strain (or where tested, the M1373A strain). Two-way ANOVA analyses yielded mutant plots of all five substrates that were significantly different from the WT.

The V1372A and I685A phenotypes are drug specific

We compared the relative resistance of these alanine-substitution mutants to the same set of five compounds used to evaluate the other alanine-substitution mutants in this study (Fig. 8). Both single mutants have striking drug-specific phenotypes. The resistance of the mutants to clotrimazole is indistinguishable from the WT (Fig. 8*A*). Relative to the WT control, both single mutants are hypersensitive to climbazole (Fig. 8*B*). The I685A mutant is also hypersensitive to tamoxifen (Fig. 8*C*) and cerulenin (Fig. 8*D*) but mildly hyper-resistant to cycloheximide (Fig. 8*E*). In contrast, the V1372A mutant is hyper-resistant to tamoxifen and cerulenin but hypersensitive to cycloheximide. The phenotype of the I685A, V1372A double mutant, however, was broader than that of the single mutants. The double mutant is hypersensitive to four of the five Pdr5 substrates; the plot of each drug follows the trajectory of the more sensitive single mutant.

An assessment of mutant hypersensitivity, however, must consider that these mutants show roughly twice the level of Pdr5 in the purified PM vesicles. Prior work clearly demonstrated that there is a linear relationship between resistance and Pdr5 expression (16). Thus, the hypersensitivity of the single and double mutants is likely underestimated. For this reason, it is probably the case that the I685A single and the I685A, V1372A double mutants are hypersensitive to all five test compounds. That said, the I685A mutant is less sensitive to climbazole and cycloheximide than it is to tamoxifen and cerulenin. Even if overexpression masks a transport-deficient phenotype, the V1372A mutant strain is no less resistant to cerulenin, tamoxifen, and possibly clotrimazole than the WT and thus also shows a drug-specific phenotype.

Table 1
Inhibition of Pdr5 ATPase activity by transport substrates

Substrate	WT	V1372A	I685A	V1372A, I685A
Clotrimazole[a]	1.17 (0.29)	1.96 (0.38)	1.78 (0.15)	6.33
Bifonazole	2.86	3.29	2.58	13.0

[a] The IC_{50} values (μM) for clotrimazole were determined from assays of two independently prepared sets of PM vesicles for WT, V1372A, and I685A. The averages and SD in parentheses are shown. Only one determination was made for the double mutant at high enough concentrations to obtain the IC_{50} (Fig. S1).

Beside Phe-683, some members of the extrusion gate region are essential for R6G transport

We assayed the mutants for their R6G transport capability against a concentration gradient of 10 μM R6G. In the first set of experiments (Fig. 9*A*), we compared the transport capability of the F1369A, G1371A, and M1373A mutants to isogenic WT and ΔPdr5 controls. As expected, the M1373A mutant (median = 4900 arbitrary units [a.u.]) was not significantly different from the ΔPdr5 strain (5001 a.u.). The F1369A mutant retained ∼5× as much fluorescence as the WT control strain (1288 a.u. *versus* 272.6 a.u.). The G1371A strain exhibited an even greater impairment (3093 a.u).

The observations regarding the relative drug resistance of the Val-1372 and Ile-685 mutant residues also apply to transport capability (Fig. 9*B*). When an unpaired t test was performed on these data, the retained R6G in the V1372A mutant was not significantly different from the WT (p = 0.330). However, both the I685A and the double I685A, V1372A mutants exhibited modest but significant increases in intracellular fluorescence (p = 0.038 and 0.016, respectively). The level of retained R6G in the double mutant was twice that of the WT strain, even though the former is overexpressed in cells.

In a second series of experiments, we compared the ability of the F1369A and G1371A mutants to transport R6G in the direction of the concentration gradient. We observed that the G1371A mutant mediated little or no R6G transport (Fig. 9*C*). The F1369A mutant, however, exhibited transport that was statistically indistinguishable from the WT in a two-way

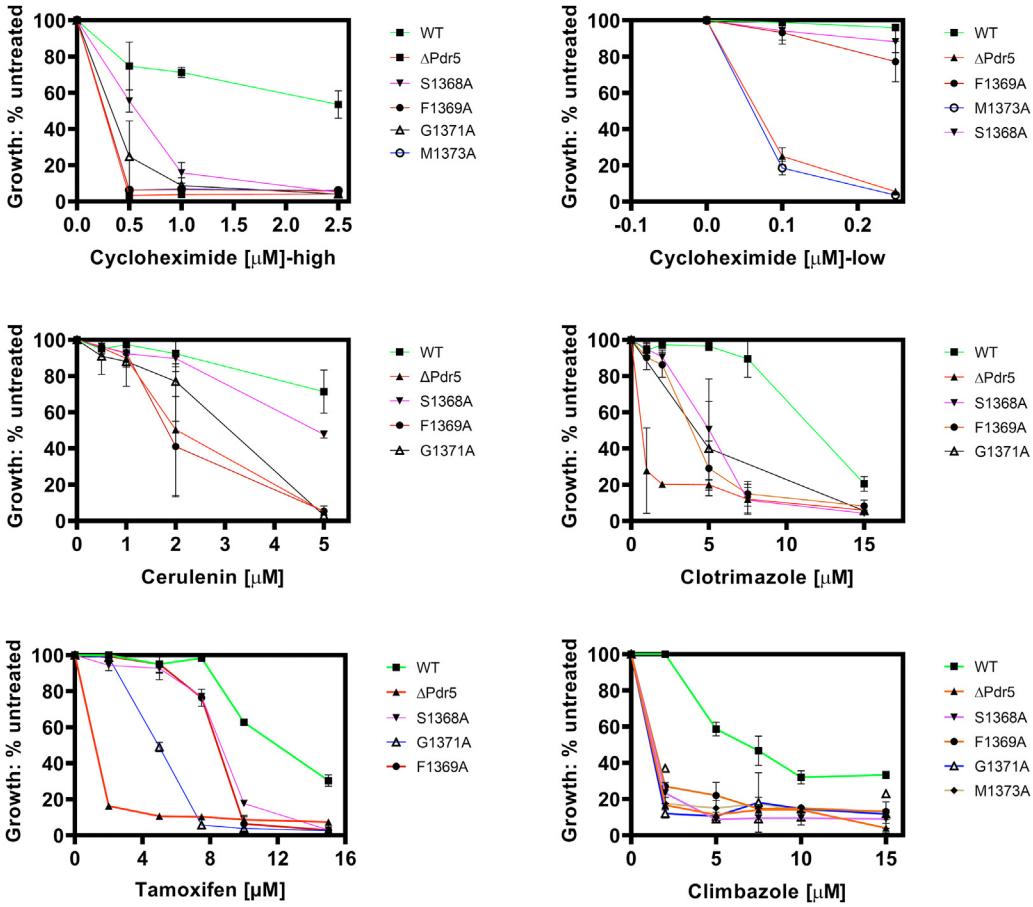

Figure 7. The F1369A and G1371A mutants exhibit profound multidrug hypersensitivity. The alanine substitution mutations were made in the pSS607 vector and placed in the ΔPdr5 strain, R-1. Resistance to five Pdr5 transport substrates was determined in liquid YPD cultures incubated for 15 h at 30 °C as described in the Experimental procedures. In these experiments, n = 3.

ANOVA test (p = 0.4807). Thus, the F1369A mutant had a phenotype like S1368A and F683L.

The molecular diode employs the same signal transmission interface used by the drug transport cycle

Biochemical analysis of the TAP antigen transporter clearly established that it contains a molecular diode requiring a functional D-loop (14) that is critical for proper signal transmission between the sites for ATP binding/hydrolysis and substrate translocation. Therefore, at least in the case of TAP, the molecular diode is dependent on the same signaling interface that is used for substrate transport.

These observations suggested that the same would very likely be true for Pdr5 and we tested this hypothesis. Furman *et al.* (23) demonstrated that a D1042N mutation in the deviant ATP-binding site D-loop greatly impaired signal transmission. Thus, although the ATPase activity approached the WT level, there was little R6G transport, and the mutant was profoundly drug hypersensitive.

We tested the ability of the D1042N mutant to exclude [^{3}H]-R6G during transport. We used the reflux assay that we originally developed to characterize the S1368A mutant (Fig. 10*A*). Cells were loaded with 10 μM nonradioactive R6G in the absence of glucose. Transport was initiated by removing the loading buffer by centrifugation and resuspending the resulting cell pellets in 20 mM Hepes–1 mM glucose buffer (pH 7.0) in the presence of 10 μM [^{3}H]-R6G. Efflux was allowed to continue for 15 min. As expected, the WT strain accumulated little [^{3}H]-R6G (median value was 0.66 ρmol/10^7). The reflux demonstrated by the D1042N mutant (median value: 4.63 ρmol/10^7 cells) was comparable to that of the ΔPdr5 strain (5.03 ρmol/10^7 cells).

The reflux studies hypothesized that in the absence of Pdr5 function, the strains would accumulate roughly the same amount of [^{3}H]-R6G through diffusion and exchange. During passive diffusion experiments in the absence of glucose, as described in Experimental procedures (Fig. 10*B*), the strains behaved similarly. These data also allowed us to calculate a drug exclusion efficiency by obtaining the ratio of [^{3}H]-R6G accumulated in Hepes-glucose buffer/[^{3}H]-R6G accumulated by passive exchange in Hepes minus glucose and subtracting that value from 100. Under these conditions, the WT strain excluded 82.3% of the [^{3}H]-R6G. The ΔPdr5 and D1042N strains failed, as expected, to exhibit a reflux barrier.

Discussion

Pdr5 is the founding member and model transporter for a large family of asymmetric, full-size ABC transporters of

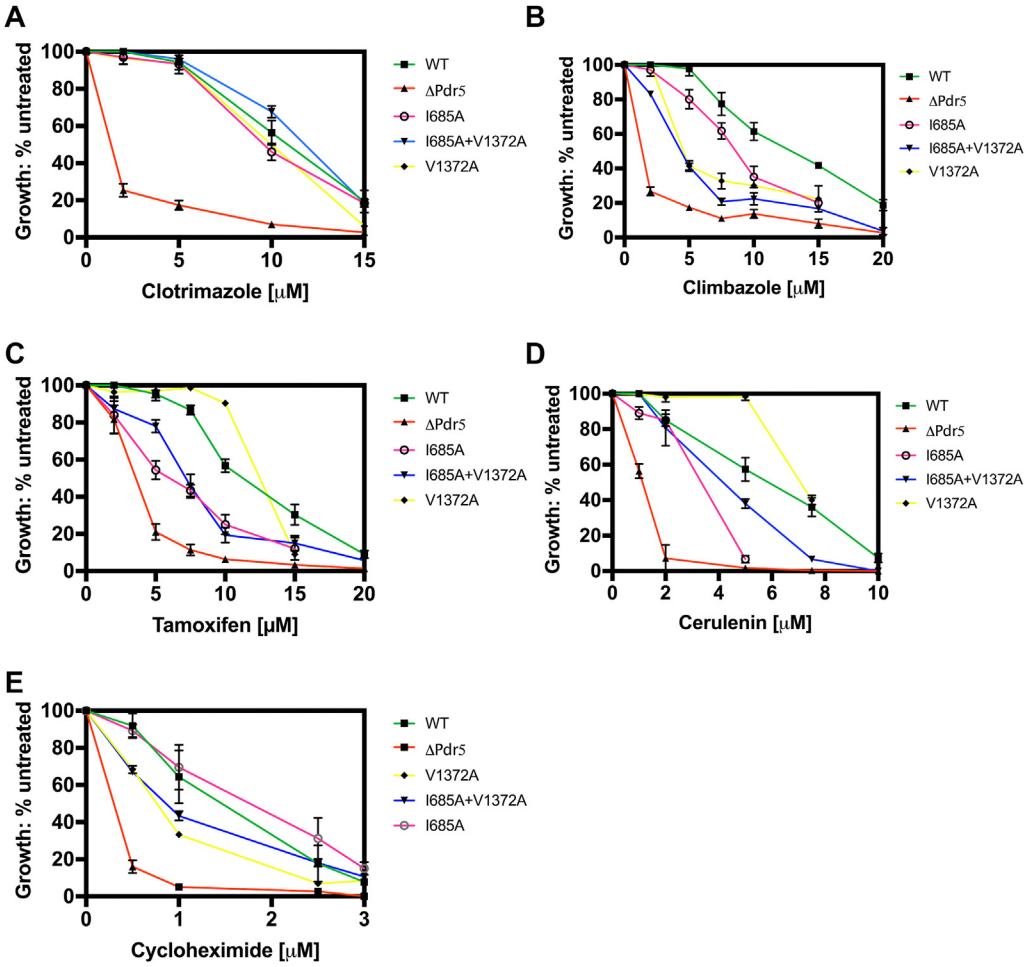

Figure 8. The I685A and V1372A mutants exhibit hypersensitivity that is drug specific. The single and double I685A and V1372A mutations were made in the pSS607 vector and placed in the ΔPdr5 strain, R-1. Resistance to five Pdr5 transport substrates (A, clotrimazole; B, climbazole; C, tamoxifen; D, cerulenin; E, cycloheximide) was determined in liquid YPD cultures incubated for 15 h at 30 °C as described in the Experimental procedures. In these experiments, n = 3.

clinically and agriculturally relevant PDR efflux pumps. The asymmetry also extends to the Pdr5 gate, which comprises four (Gly-682, Phe-683, Gly-1371, and Met-1373) rather than six residues found in the symmetric mammalian transporter ABCG2.

This study is the first to look systematically at the function of residues in the region of the extrusion gate of an ABC transporter. Eleven single and one double mutant were either isolated or constructed. The major phenotypic features of most of the mutants are listed in Table 2. As was the case with its ABCG2 equivalent, L555A, the M1373A mutant is absent from the membrane. This suggests that in addition to its role as part of the hydrophobic plug in both transporters, this highly conserved residue may be critical for protein folding or membrane localization.

When the F683L mutation is modeled *in silico*, it fails to contact Met-1373, a potential leak is created, and reflux of transport substrates can occur. This explains the general hypersensitivity of the mutant and its transport deficiency against a concentration gradient of R6G. Thus, the phenotype of the F683L mutant closely resembles that of both S1368A and F1369A. In the cryo-EM structures, Phe-1369 interacts with the gate residue Gly-1371 and with Ser-1366 and Leu-1367. Ser-1368 interacts with Met-1373 (see later), Thr-1364, and Met-1365. Ser-1368 and Phe-1369 appear to be essential members of a residue network that also includes the gate residues.

The M1373T interchange mutant represents a striking substitution of a smaller polar residue. Nevertheless, its phenotype is milder than the F683L. When the threonine mutation is created *in silico*, an interaction suddenly occurs with the backbone carbonyl of Ser-1368, which may be partly compensatory.

The V1372A, A684S, and I685A mutants are on opposite sides of the channel and the corresponding WT residues do not participate in gate formation. Nevertheless, these mutants have two important and interesting features. The first is their drug specificity. Relative to the WT control, the I685A mutant is less sensitive to climbazole and cycloheximide than it is to tamoxifen or cerulenin. The V1372A mutant has almost the opposite phenotype. It is more resistant to tamoxifen and cerulenin than it is to climbazole and cycloheximide. The double mutant has the phenotype of the more sensitive single mutant. The A684S mutant also

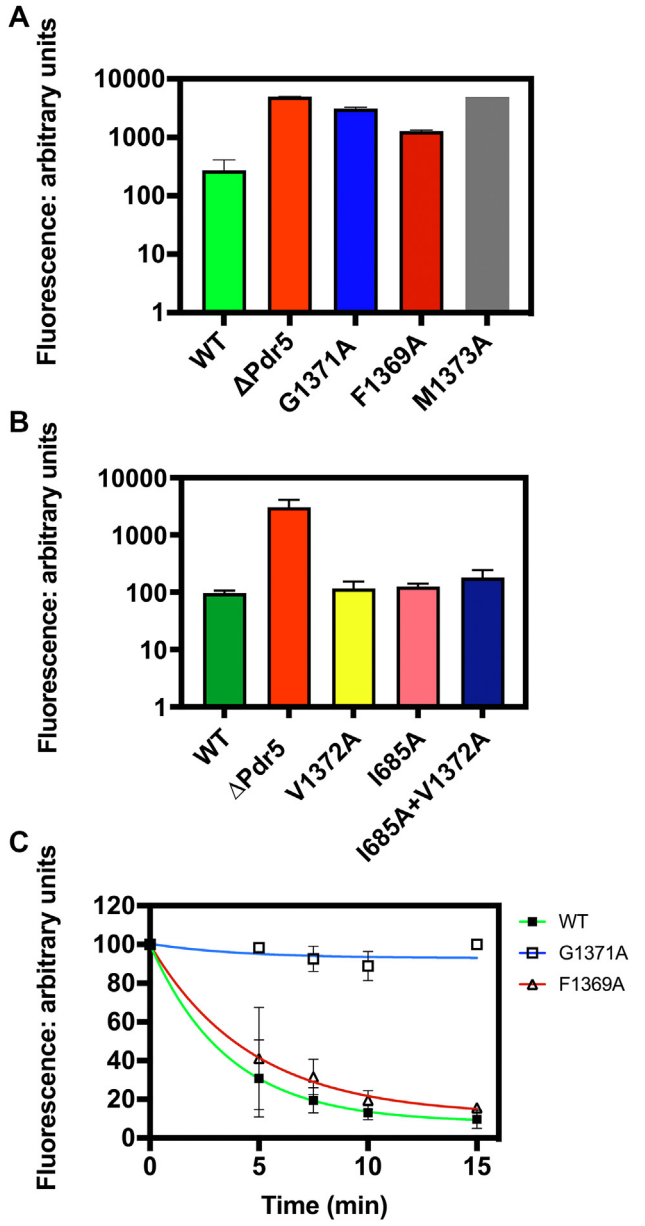

Figure 9. The F1369A and G1371A mutants have distinguishable transport phenotypes. *A* and *B*, R6G transport against a concentration gradient of 20 μM R6G was assayed as described in the Experimental procedures. In these experiments, n ≥ 4. *C*, the transport capability of the F1369A and G1371A mutants in the direction of 20 μM R6G was measured as described in the Experimental procedures. In these experiments, n = 3. R6G, rhodamine 6G.

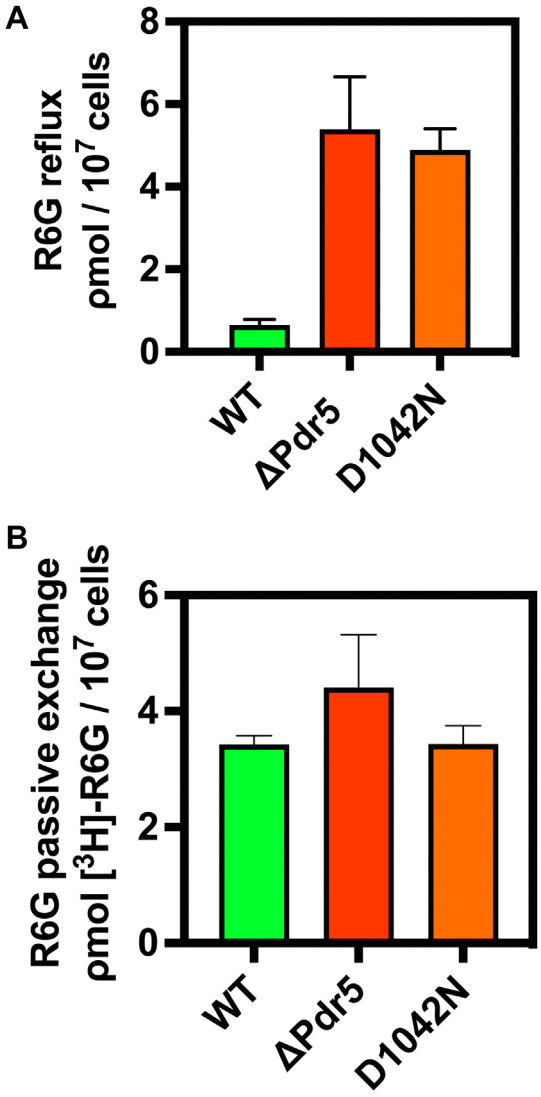

Figure 10. The Pdr5 extrusion gate relies on the same signal transmission interface as drug transport. *A*, reflux assay was performed as described in the Experimental procedures. WT cells and cells containing a D1042N mutation were preloaded with 10 μM of R6G at 30 °C for 90 min in 0.02 M Hepes buffer (pH 7.0) minus glucose before resuspension in 0.02 Hepes, 1 mM glucose buffer (pH 7.0) containing 10 μM [^{3}H]-R6G. Transport proceeded at 30 °C for 15 min. *B*, passive isotope exchange experiments in the absence of glucose were performed as described in the Experimental procedures. In these experiments, n = 3. R6G, rhodamine 6G.

exhibits drug specificity. Although it is sensitive to cycloheximide, ketoconazole, and fluconazole, this mutant exhibits a WT level of resistance to R6G. These data suggest that Val-1372, Ala-684, and Ile-685 interact with transport substrates as they exit and are required for successful efflux through the narrow channel. These features, along with the proximity of the gate to the substrate-binding pocket, suggest an alternative explanation for the extraordinary cooperativity that is observed during R6G transport (21). Heretofore, it was assumed that this represented binding of R6G molecules at multiple places in the drug-binding pocket. However, only a single bound R6G molecule was observed in the cryo-EM images. Alternatively, it is plausible that binding in the drug pocket enhances subsequent interaction with the channel residues. In any event, the density of R6G in the cryo-EM structures is not as defined as the protein density. This implies some positional flexibility and thus different modes of drug binding.

Further evidence that Val-1372 and Ile-685 interact with drugs comes from the observation that the ATPases from V1372A and I685A single mutants and the double I685A, V1372A mutant are hyper-resistant to allosteric inhibition. Furthermore, the nonadditivity of the double mutant IC_{50} indicates that although these residues are on opposite sides of the channel, they are part of the same allosteric site.

Table 2
Major phenotypic features of the gating region mutants

Mutant[a]	Drug specific?	ATPase activity	R6G transport against/with gradient deficient?	Sensitivity to allostery
S1368A[b]	No	WT	Yes/No	WT
F1369A	No	WT	Yes/No	WT
F683L	No	WT	Yes/No	WT
M1373T	Yes	WT	ND[c]	WT
A684S	Yes	WT	ND	WT
V1372A	Yes	WT	No/No	hyperresistant
I685A	Yes	WT	Yes[d]/ND	hyperresistant
G1371A	No	Reduced	Yes/Yes	hypersensitive

[a] The G682A and M1373A mutant proteins are absent from PM vesicles and these mutants are not listed.
[b] Data are from Mehla *et al.* (13).
[c] Not determined.
[d] Very mild, but statistically significant.

We suggest that allosteric inhibition is an SOS mechanism, as proposed by Gupta *et al.* (9). Once the extracellular concentration of a substrate is relatively high (perhaps because of transporter-mediated efflux), the possibility of reflux *via* the binding residues of the transporter increases. Inhibition of the ATPase activity stops the transport cycle and thus reentry is limited to slower, passive diffusion. Transport substrate inhibition of ATPase activity has been documented with other eukaryotic ABC efflux transporters, including P-gp, ABCG2, and Cdr1 (24–26). In the two mammalian transporters, the same substrates that stimulate ATPase at low concentrations are inhibitors at high concentration. The mechanism by which P-gp is allosterically inhibited was recently elucidated (26). In the ABCG2 transporter, the site of inhibitor action appears to be the binding pocket (27), where it locks the protein in an IF conformation (28). The drug-binding sites and inhibitory sites overlap (29). The structural basis of allosteric inhibition was also determined for two bacterial transporters. In the case of the molybdate/tungstate transporter from *Methanosarcina acetivorans* (30), the allosteric site is in the NBD regulatory region. Binding of two molecules at two oxyanion sites locks this importer in the IF conformation. The location of an allosteric inhibition site for the *Escherichia coli* methionine transporter was also determined (31). This importer has a carboxyl terminal extension. Binding of methionine in this region prevents nucleotide dimerization. These studies strongly suggest that ABC transporters use an array of different mechanisms to achieve inhibition by their transport substrates.

Among the nine single mutants that we analyzed, the G1371A phenotype is unique. Although Gly-1371 is part of the Pdr5 gate, the G1371A mutant, in striking contrast to the F1369A, F683L, and S1368A mutants, exhibits a severe transport defect with and against an R6G concentration gradient. The mutant also has reduced ATPase activity, and what remains is also strikingly hypersensitive to allosteric inhibition by clotrimazole and bifonazole. The mutant behavior is consistent with the presence of a residue required for the switch from the IF to the OF conformation. The position of Gly-1371 in the IF and OF conformations is illustrated in Fig. S7. In the IF conformation, Gly-1371 has a phi/psi combination of approximately +120/+5. This corresponds to a residue in a left-handed alpha helix in a Ramachandran plot. However, in the OF structure, the phi/psi combination changes to approximately +70/-170, a region in the Ramachandran plot in which only glycine residues are permitted. Thus, we suggest that the mutation of G1371 to A impairs the arrangement of this area and slows the switch from the IF to the OF conformation. However, while the resolution of the IF, R6G-bound state is 3.1 Å the resolution of the OF state is only 3.9 Å. Although this hypothesis requires experimental validation of Pdr5 structures at higher resolution, it is consistent with the observation that in alignments with other PDR subfamily members, this glycine is 99% conserved. A high level of conservation also appears in the ABCG subfamily. This hypothesis also explains the increased sensitivity of the G1371A mutant to allosteric inhibition. We posit that per unit time, fewer molecules of the G1371A mutant are in the OF conformation, where ATP hydrolysis takes place (6). Therefore, relative to the WT enzyme, a lower concentration of an allosteric inhibitor such as clotrimazole would achieve complete inhibition of ATPase activity. It is also clear that Gly-1371 plays a central role in creating the loop where this essential residue resides. We suspect this residue plays an analogous role throughout the large PDR and ABCG subfamilies.

We initially considered a role for Gly-1371 in signal transmission. This appears unlikely. While some mutants in the signal interface exhibit reduced ATPase activity, their loss of signal generally makes enzyme activity hyper-resistant to allosteric inhibition rather than hypersensitive (19, 20).

Bioinformatic analysis indicated that the highly conserved Gly-682 residue in the amino terminal half of Pdr5 aligns with Gly-1371. Phenotypically, however, the G1371A and G682A mutants are quite different, as the latter mutant protein is not found in the PM. The phi/psi values for Gly-682 are +100/+5 for the IF conformation and therefore like Gly-1371. During the switch to the OF conformation, however, the Gly-682 values barely change (+110/-5). This is because the amino terminal half of Pdr5 moves very little during the IF to OF transition. It is likely, therefore, that the Gly-682 residue is essential for proper protein folding and trafficking to the PM.

In summary, Pdr5 is asymmetric in its gating function. Gly-682, Phe-683, Gly-1371, and Met-1373 make up the gate proper. Phe-683 and Met-1373 create a hydrophobic barrier, and Gly-1371 appears to be required for conformational switching. Ser-1368 and Phe-1369 are part of an essential network of residues that interact with the gate proper, and alanine substitutions in these are phenotypically similar to the F683L mutant (Table 2). Instead of participating in gate closure, Ile-685 and Val-1372 are part of an allosteric site. We suggest that this provides an alternate means of preventing reflux.

Experimental procedures

Construction of cryo-EM structures

Figures 2 and 3 were constructed in Pymol (www.pymol.org) with the single-molecule cryo-EM structures that were previously reported (6).

Strains and plasmids

All yeast strains used in this study are listed in Table S2 and most are derived from R-1, a strain lacking the major PM ABC transporters, including Pdr5. R-1 is a derivative of and closely related to AD1-7 (19). To make R-1 from AD1-7, the *URA3* insertion was removed by selection of 5-fluoroorotic acid (5-FOA) resistant colonies. As a result, these colonies were rendered *ura3*. Following this, one of these colonies was retained and the entire coding region of *PDR5* was replaced in by a *KanMX4* cassette by genetic transformation. This genetic background offers numerous other advantages for genetic and biochemical analyses, described in detail elsewhere (5). Culturing of strains was carried out at 30 °C. The pSS607-integrating plasmid (19) was used for site-directed mutagenesis and gene replacement as previously described (5). This plasmid has a WT *PDR5* gene under the transcriptional control of its own promoter region as well as a *URA3*-selectable marker. Our WT positive control strain (JG2015) was constructed by placing this plasmid in R-1. We grew our strains in yeast extract, peptone, dextrose medium at 30 °C.

Chemicals and media

All chemicals were purchased from Sigma–Aldrich, except for 5-FOA and G-418, from Research Products International, and cerulenin, from LKT laboratories. All chemicals were dissolved in dimethyl sulfoxide except for 5-FOA and G-418, which were dissolved in sterilized SD+ his and yeast extract, peptone, dextrose medium, respectively. We purchased [^{3}H]-R6G (1.5 and 0.4 Ci/mol) from Moravek Radiochemicals.

Measurement of relative drug resistance

We determined the relative resistance of alanine-substitution mutant strains to clotrimazole, cycloheximide, and cerulenin with the isogenic ΔPdr5 (R-1) and WT (JG2015) strains serving as controls. We placed 2 ml YPD broth in sterile glass tubes. To the first tube, 5 μl of drug stock solution (5 mM) was added. The desired concentration of drug was introduced as a 2-fold dilution into the tubes and 0.5 × 10^5 cells (typically 2–5 μl) were added. The tubes were incubated for 24 h, and the absorbance was measured at 600 nm (A_{600}). From the A_{600} data, the percent inhibition (%I) was calculated as follows: %I = 1 - (Ac/Ao) × 100, where Ac is the A_{600} of the culture at a given concentration of drugs and Ao is the A_{600} of the positive control. The relative resistance of the FK506-resistant mutants was measured by the method reported in Gupta *et al.* (32).

Site-directed mutagenesis

Alanine substitution mutations were introduced into pSS607 with a Quikchange Lightning site-directed mutagenesis kit (Life Technologies). Mutant primers were designed with a genomics program provided by Agilent Technologies. The primers were purchased from integrated DNA technologies. The mutant plasmids were introduced into XL-Gold *E. coli* by transformation, as described in the Quikchange instruction manual. Plasmid DNA was extracted from the transformants with an IBI miniprep kit and sequenced commercially to confirm the presence of the mutation in the plasmid. The mutant plasmid DNA was introduced into R-1 with a Sigma–Aldrich yeast transformation kit. Genetic testing confirmed that the construct was correctly inserted, as described by Ananthaswamy *et al.* (5).

Preparation of purified PM vesicles

We adopted the procedure of Kolaczkowski *et al.* (21) with minor modifications (8).

Gel electrophoresis and Western blotting of PM vesicle proteins

The amount of Pdr5 in PM vesicles of the F683L, A684S, and M1373T mutants (Fig. 4) was evaluated with 10 μg of PM vesicle protein (solubilized in SDS-PAGE sample buffer, heated to 65 °C for 10 min) were separated by electrophoresis at 80 to 120 V on 7% acrylamide gels before transferring to a polyvinylidene difluoride membrane (0.45 μm, Amersham Hybond) at constant current (25 V, 30 min) in a Bio-Rad Trans-Blot Turbo Transfer System. The membranes were blocked overnight in blocking solution (10% milk powder, 0.05% sodium azide [Sigma] in Tris-buffered saline [TBS], 0.1% Tween 20 [TBS-T]). After blocking, the blots were washed three times for 10 min in TBS-T. The Pdr5-specific primary antibody (Karl Kuchler, Vienna) was diluted 1:3000 in TBS-T substituted with 3% bovine serum albumin. The blots were incubated in the primary antibody for 1 h at room temperature (RT) under gentle agitation. Before addition of the secondary antibody, the blots were washed three times for 10 min in TBS-T. The secondary antibody (goat, anti-rabbit IgG whole-molecule peroxidase antibody, Sigma) was diluted 1:10,000 in TBS-T and substituted with 5% milk powder. The blots were incubated at RT for 1 h under gentle agitation. Before developing, the blot was washed twice for 10 min in TBS-T and once for 10 min in TBS. The blots were developed with a WESTAR ηC Ultra 2.0 chemiluminescent substrate kit (Cyanagen) and the signals detected with an Amersham Imager 680.

For analysis of the alanine-substitution mutants (Fig. 7), we followed a previously described gel electrophoresis protocol (33). We solubilized samples containing 5 μg PM vesicle protein in SDS-PAGE for 30 min at 37 °C. We separated the proteins on NU PAGE 7% tris acetate gels (125–150 V) for ∼80 min (Life Technologies). Gels were stained with SimplyBlue (Coomassie blue-250 safe stain). Densitometry of the gel bands was performed with ImageJ software (imagej.nih.gov).

We conducted Western blotting with 5 μg PM vesicle protein separated by gel electrophoresis as previously described (33).

Assay of ATPase activity

We measured Pdr5-specific ATPase activity for 8 min at 35 °C with 2 μg purified PM vesicle protein in Tris-glycine (pH 9.5) buffer as previously described (8, 33). The non-Pdr5

activity observed in the ΔPdr5 negative control strain was subtracted as the background before calculating the activity. Two independent PM vesicle preparations were made for each mutant, and two determinations of enzyme activity were performed with each preparation. Western blots were also performed with each set of PM vesicles.

R6G transport in purified PM vesicles

Fluorescence quenching of R6G in PM vesicles was performed as previously described (8). Each reaction contained 30 μg purified PM vesicle protein, 5 mM ATP, 5 mM Mg^{2+}, and 150 nM R6G.

Whole-cell, nonradioactive R6G transport assays

Two different transport assays with nonradioactive R6G were used in this study. In the first, we measured R6G transport against a 10 μM concentration gradient. We placed 3 × 10^6 cells in 500 μl 0.02 M Hepes, 1 mM glucose (pH 7.0) buffer containing 20 μM R6G, and incubated them at 30 °C for 90 min. The cells were collected by microcentrifugation and washed with 1 ml cold 0.02 M Hepes buffer (pH 7.0) minus glucose. The pellets were resuspended in 500 μl of the same buffer and analyzed with a fluorescence activated cell sorter whose laser had an excitation wavelength of 529 nm and an emission wavelength of 553 nm. For each determination, the median retained fluorescence was obtained from sorting 10,000 cells. We analyzed the data with a CellQuest program. We expressed retained fluorescence in arbitrary units.

We also measured R6G transport in the direction of a concentration gradient. We loaded 3 × 10^6 exponentially dividing cells with R6G. We suspended them in 100 μl 0.02 M Hepes buffer (pH 7.0) minus glucose for 90 min in the presence of 20 μM R6G. Following loading, cells were collected by microcentrifugation and the supernatant removed before resuspending in 500 μl 0.02 M Hepes (pH 7.0) plus 1 mM glucose. We incubated the tubes at 30 °C for a desired time. We terminated transport reactions by placing the tubes in an ice water bath. We determined cell fluorescence as described before.

Measurement of [^{3}H]-R6G reflux

Reflux of 20 μM [^{3}H]-R6G during transport was measured as first described by Mehla *et al.* (13). Cells were grown and 5 × 10^6 were preloaded in 500 μl of 20 μM R6G in the absence of glucose as described before. Following this, the cells were pelleted by microcentrifugation (1 min, 15,000 rpm), the supernatant was discarded, and the pellets were resuspended in 500 μl 0.02 M Hepes buffer (pH 7.0) containing 1 mM glucose and 20 μM [^{3}H]-R6G. Cells were incubated for 15 min at 30 °C. Transport was terminated by placing the reaction tubes in an ice water bath. The cells were pelleted at 4 °C and the supernatants were discarded. The cells were washed 3× with 1 ml of ice cold 0.02 M Hepes buffer (pH 7.0) minus glucose. The radioactivity remaining in the cells was determined by scintillation counting in a TriAthler liquid scintillation counter (Lab Logic). Passive exchange experiments were performed with the same protocol except that cells were resuspended in Hepes buffer containing 20 μM [^{3}H]-R6G but no glucose.

Statistical analyses

Statistical analyses were performed with Prism Graphpad software (GraphPad Software Inc). Unless otherwise indicated, the error bars represent the mean with the standard error.

Bioinformatic analyses

Alignments between ABC transporters were made with the ExPASy database (https://www.expasy.org/).

Data availability

All data are included in the main text or as two tables and four figures in the Supporting Information.

Supporting information—This article contains supporting information (34).

Acknowledgments—We thank Nathan Kelsey and Jaesen Evangelista for their excellent research assistance. As usual, Trish Weisman made numerous useful editorial suggestions and corrections.

Author contributions—M. A., L.- M. N., H. R., L. S., A. R., A. H., C. D., L. R., E. L., N. A., S. V. A., J. S. C., and J. G. data curation and/or writing – review & editing. M. A., L.- M. N., H. R., A. R., C. D., N. A., L. R., J. G., and A. H. investigation. L. S. methodology. J. C. and S. V. A. resources.

Funding and additional information—This work was supported by NIH grant GM07721 to J. G. Research by L. S. is funded by the DFG (grant Schm1279/17-1). Work by S. V. A. is supported by the Intramural Health, NIH, National Cancer Institute, Center for Cancer Research. A. S.-H. was funded through ERC Advanced grant VisTrans (ID: 742210). The content is solely the responsibility of the authors and does not necessarily represent the official views of the National Institutes of Health.

Conflict of interest—The authors declare that they have no conflicts of interest with the contents of this article.

Abbreviations—The abbreviations used are: 5-FOA, 5-fluoroorotic acid; a.u., arbitrary unit; IF, inward-facing; NBD, nucleotide-binding domain; OF, outward-facing; PM, plasma membrane; R6G, rhodamine 6G; TBS, Tris-buffered saline; TBS-T, TBS 0.1% Tween 20; TMD, transmembrane-binding domain.

References

1. Hofmann, S. H., Januliene, D., Mehdipour, A. R., Thomas, C., Brucher, S., Kuhn, B. T., *et al.* (2019) Conformation of a heterodimeric ABC exporter under turnover conditions. *Nature* **571**, 580–583
2. Thomas, C., and Tampe, R. (2020) Structure and mechanistic principles of ABC transporters. *Ann. Rev. Biochem.* **86**, 605–636
3. Manolaridis, I., Jackson, S., Taylor, N., Kowal, N., Stahlberg, H., and Locher, K. P. (2018) Cryo-EM structures of a human ABCG2 mutant trapped in ATP-bound and substrate-bound states. *Nature* **563**, 426–430
4. Lee, J.-Y., Kinch, L. M., Borek, D. H., Wang, D. J., Wang, J., Urbatsch, I. L., *et al.* (2016) Crystal structure of the human sterol transporter ABCG5/ABCG8. *Nature* **533**, 561–564

5. Ananthaswamy, N., Rutledge, R., Sauna, Z. E., Ambudkar, S. V., Dine, E., Nelson, E., *et al.* (2010) The signaling interface of the yeast multidrug transporter Pdr5 adopts a cis configuration and there are functional overlap and equivalence of the deviant and canonical Q- loop residues. *Biochemistry* **49**, 4440–4449
6. Harris, A., Wagner, M., Du, D., Raschka, S., Gohlke, H., Smits, S. H. J. V., *et al.* (2021) Structure and efflux mechanism of the yeast pleiotropic drug resistance transporter Pdr5. *Nat. Commun* **12**, 5254
7. Golin, J., and Ambudkar, S. V. (2015) The multidrug transporter Pdr5 on the 25th anniversary of its discovery: an important model for the study of asymmetric ABC transporters. *Biochem. J.* **467**, 353–363
8. Ernst, R., Kueppers, P., Klein, C. M., Schwarzmueller, T., Kuchler, K., and Schmitt, L. (2008) A mutation of the H-loop selectively affects rhodamine transport by the yeast multidrug transporter Pdr5. *Proc. Natl. Acad. Sci. U. S. A.* **105**, 5069–5074
9. Higgins, C. F., and Gottesman, M. M. (1992) Is the multidrug transporter a flippase? *Trends Biochem. Sci.* **17**, 18–21
10. Raschka, S. L., Harris, A., Luisi, B. F., and Schmitt, L. (2022) Flipping and other astonishing transporter dance moves in fungal drug resistance. *Bioessays* **4**, e2200035
11. Sauna, Z. E., and Ambudkar, S. V. (2000) Evidence for a requirement for ATP hydrolysis at two distinct steps during a single turnover of the catalytic cycle of human P-glycoprotein. *Proc. Nat. Acad. Sci. U. S. A.* **97**, 2515–2520
12. Gupta, R. P., Kueppers, P., Schmitt, L., and Ernst, R. (2011) The multidrug transporter Pdr5, a molecular diode? *Biol. Chem.* **391**, 53–60
13. Mehla, J., Ernst, R., Moore, R., Wakschlag, A., Marquis, M. K., Ambudkar, S. V., *et al.* (2014) Evidence for a diode-based mechanism in a multispecific ATPbinding cassette (ABC) transporter Pdr5. *J. Biol. Chem.* **289**, 26597–26606
14. Grossmann, N., Vakkasoglu, A. S., Hulpke, S., Abele, R., Gaudet, R., and Tampé, R. (2014) Mechanistic determinants of the directionality and energetics of active export by a heterodimeric ABC transporter. *Nat. Commun.* **5**, 5419
15. Lamping, E., Baret, P. V., Holmes, A. R., Monk, B. C., Goffeau, A., and Cannon, R. (2010) Fungal PDR transporters: Phylogeny, topology, motifs, and function. *Fungal Genet. Biol.* **47**, 127–142
16. Golin, J., Ambudkar, S. V., Gottesman, M. M., Habib, A. D., Sczepanski, J., Ziccardi, W., *et al.* (2003) Studies with novel Pdr5 substrates demonstrate a strong size dependence for xenobiotic efflux. *J. Biol. Chem.* **278**, 5963–5969
17. Tanabe, K., Bonus, M., Tomiyama, S., Miyoshi, K., Nagi, M., Niimi, K., *et al.* (2019) FK506 resistance of *Saccharomyces cerevisiae* Pdr5 and *Candida albicans* Cdr1 involves mutations in the transmembrane domains and extracellular loops. *Antimicrob. Agent Chem.* **63**. https://doi.org/10.1128/AAC.01146-18
18. Golin, J., Kon, Z. N., Wu, C. P., Martello, J., Hanson, L., Supernavage, S., *et al.* (2007) Complete inhibition of the Pdr5 multidrug efflux pump ATPase activity by its transport substrate clotrimazoletrimazole suggests GTP as well as ATP may be used as an energy source. *Biochemistry* **46**, 13109–13119
19. Sauna, Z. E., Bohn, S. S., Rutledge, R., Dougherty, M. P., Cronin, S., May, L., *et al.* (2008) Mutations define crosstalk between the N-terminal nucleotide-binding domain and transmembrane helix-2 of the yeast multidrug transporter Pdr5. Possible conservation of a signaling interface for coupling ATP hydrolysis and drug transport. *J. Biol. Chem.* **283**, 35010–35022
20. Downes, M. T., Mehla, J., Ananthaswamy, N., Wakschlag, A., LaMonde, M., Dine, E., *et al.* (2013) The transmembrane interface of the Saccharomyces cerevisiae multidrug transporter Pdr5: Val-656 located in intracellular-loop 2 plays a major role in drug resistance. *Antimicrob. Agents Chemother.* **57**, 1025–1034
21. Arya, N., Rahman, H., Rudrow, A., Wagner, M., Ambudkar, S. V., and Golin, J. (2019) An A666G mutation in transmembrane helix 5 of the yeast multidrug transporter Pdr5 increase drug efflux by enhancing cooperativity between transport sites. *Mol. Microbiol.* **112**, 1131–1144
22. Kolaczkowski, M., van der Rest, M., Cybularz-Kolaczkowski, A., Soumillion, J.-P., Konings, W. N., and Goffeau, A. (1996) Anticancer drugs, ionophoric peptides and steroids as substrates of the yeast multidrug transporter Pdr5. *J. Biol. Chem.* **271**, 31543–31548
23. Furman, C., Mehla, J., Ananthaswamy, N., Arya, N., Kulesh, B., Kovach, I., *et al.* (2013) The deviant ATP-binding site of the multidrug efflux pump Pdr5 plays an active role in the transport cycle. *J. Biol. Chem.* **288**, 30420–30431
24. Jani, M., Maki, I., Kis, E., Szabo, P., Nagy, T., Krajcs, P., *et al.* (2011) Ivermectin interacts with human ABCG2. *J. Pharm. Sci.* **100**, 94–97
25. Litman, T., Zeuthen, T., Skovagaard, T., and Stein, W. D. (1997) Competitive, non-competitive, and cooperative interactions between substrates of P-glycoprotein as measured by its ATPase activity. *Biochim. Biophys. Acta Biomembr.* **1361**, 169–176
26. Dastvan, R., Mishra, S., Peskova, Y. B., Nakamoto, R. K., and Metlauorab, H. S. (2019) Mechanism of allosteric modulation of P-glycoprotein by transport substrates and inhibitors. *Science* **264**, 689–693
27. Jackson, S. M., Manolardis, I., Kowal, J., Zechner, M., Taylor, N. M. I., Bauer, M., *et al.* (2018) Structural basis of small-molecule inhibition of human multidrug transporter ABCG2. *Nat. Struct. Mol. Biol.* **25**, 333–340
28. Srikant, S., and Gaudet, R. (2019) Mechanics and pharmacology of substrate selection and transport by eukaryotic ABC transporters. *Nat. Struct. Mol. Biol.* **26**, 792–801
29. Lusvarghi, S., and Ambudkar, S. V. (2019) ATP-dependent thermostabilization of human P-glycoprotein (ABCB1) is blocked by modulators. *Biochem. J.* **24**, 3737–3750
30. Gerber, S., Comellas-Bigler, M., Goetz, B., and Locher, K. P. (2008) Structural basis of transinhibition in a molybdate/tungstate ABC transporter. *Science* **321**, 246–250
31. Kadaba, N. S., Kaiser, J. T., Johnson, E., Lee, A., and Rees, D. C. (2008) The high affinity *E. coli* methionine ABC transporter: structural and allosteric regulation. *Science* **321**, 250–253
32. Gupta, R. P., Kueppers, P., Hanekop, N., and Schmitt, L. (2014) Generating symmetry in the asymmetric ATP-binding cassette (ABC) transporter Pdr5 from. *Saccharomyces Cerevisiae. J. Biol. Chem.* **289**, 15272–15279
33. Rahman, H., Rudrow, A., Carneglia, J., Joly, S. S. P., Nicotera, D., Naldrett, M., *et al.* (2020) Nonsynonymous mutations in linker-2 of the Pdr5 multidrug transporter identify a new RNA stability element. *G3 (Bethesda)* **10**, 351–369
34. Lamping, E., Monk, B. C., Niimi, K., Holmes, A. R., Tsao, S., Tanabe, K., *et al.* (2007) Characterization of three classes of membrane proteins involved in fungal azole resistance by functional hyperexpression in. *Saccharomyces Cerevisiae. Eukaryot. Cell* **6**, 1150–1165